Chemical Engineering & Processing: Process Intensification 226 (2026) 110868

Contents lists available at ScienceDirect

Chemical Engineering and Processing - Process Intensification

journal homepage: www.elsevier.com/locate/cep

Numerical investigation of flow reverser effects on thermal and hydraulic performance of a rotating horizontal spiral coil heat exchanger

Mohammad Mobin Bakhshi [a,*], Faezeh Ahangar [a,b], Ganesh Desai Ramakrishna [a], Huixuan Wu [a], Wei Guo [a,b]

[a] Mechanical Engineering Department, FAMU-FSU College of Engineering, Tallahassee, FL 32310, USA
[b] National High Magnetic Field Laboratory, 1800 East Paul Dirac Drive, Tallahassee, FL 32310, USA

ARTICLE INFO

Keywords:
Spiral coil heat exchanger
Flow reverser
Dean vortices
Thermohydraulic performance
Computational Fluid Dynamics
Heat transfer enhancement

ABSTRACT

This study numerically investigates a rotating horizontal spiral tube heat exchanger with integral flow-reversal segments designed to enhance thermohydraulic performance. As opposed to the typical spiral coil heat exchanger where the effect of Dean vortices gradually diminishes along the flow direction, an innovative configuration is introduced here where the motion of the Dean vortices can be re-created periodically through flow reversal. Three-dimensional computational fluid dynamics analysis was carried out using the concept of rotating reference frame to examine the fluid flow and heat transfer properties for the range of Reynolds number 2000 to 6000, which corresponds to the laminar to transitional flows in curved tubes. It was found that, relative to a conventional horizontal spiral coil, there is an improvement in Nusselt number of 16.3%, 26.8%, and 32.9% at Reynolds numbers of 2000, 4000, and 6000, respectively. The pressure drop penalty is about 6.7%, 17.9%, and 12.6% at Reynolds numbers of 2000, 4000, and 6000, respectively. These results demonstrate that geometric modification through periodic flow reversal can significantly enhance heat transfer without the need for internal inserts. The proposed configuration provides an efficient, manufacturable, and energy-efficient solution for industrial applications such as desalination, cooling, and waste heat recovery.

1. Introduction

In many engineering applications, including power generation, refrigeration, transportation, heat exchangers play a crucial role in controlled heat transfer between fluid streams. An efficient heat exchanger becomes important for cost reduction and conservation of heat [1,2]. Improving the efficiency of thermal systems is directly linked to reducing energy consumption and supporting resource management [3]. In order to meet the increasing needs of strict environmental regulations and demand, there lies an intensive need for miniature, robust, and environment-friendly design that would provide superior heat transfer rates [4].

Heat transfer enhancement techniques are broadly grouped into two categories: passive and active. Passive methods include the use of different materials and geometry, for example, the introduction of fins [5]. Passive approaches include material and geometric variations, such as finned surfaces [6], wavy and curved passages [7], and surface roughening, as well as insertion devices like wire coil [8] and twisted tape insertions [9]. Recent studies have demonstrated the effectiveness of such passive techniques. For instance, Zhang et al. (2025) showed that coiled wire inserts in spiral channels significantly improve secondary flow intensity and heat transfer efficiency by increasing flow instability [10]. Similarly, Qiu et al. (2025) studied an innovative I-rib twisted tape and twisted winglet (I-RTTW) arrangement, which incorporates edge winglets for boundary layer disruption and central I-ribs for radial momentum transport. It was found that for constant Reynolds numbers, increasing wing depth ratio and wing width ratio result in improved heat transfer efficiency and higher flow resistance; in particular, Nusselt number is 1.78–1.99 times higher than that for a smooth tube, whereas the friction factor is 3.76–4.11 times greater [11]. Heat transfer enhancement in passive methods is primarily achieved through boundary layer disruption and intensified fluid mixing, which increase convective heat transfer coefficients [12]. Various geometric modifications have been investigated to achieve this effect. For example, Pei et al. (2025) developed a highly efficient cooling technique for high-end electronic products using counter-flow microchannel with sinusoidal

* Corresponding author.
E-mail address: mb23da@fsu.edu (M.M. Bakhshi).

https://doi.org/10.1016/j.cep.2026.110868
Received 5 December 2025; Received in revised form 19 April 2026; Accepted 11 May 2026
Available online 13 May 2026

wave walls. The use of sinusoidal wave walls in the system helps enhance its efficiency by increasing the heat transfer area while enhancing the efficiency of film evaporation. The efficiency of heat transfer was improved by 103 % in comparison with traditional microchannel techniques [13]. Alzaben et al. (2025) showed that the introduction of spring wire inserts into a double-tube heat exchanger influences the heat transfer characteristics. The major influence noted in the results obtained is the ratio of pitch length, which had an optimum value of 1.03 and which increased the Nusselt number with an improvement of 184 % to 194 % when compared with the plain tube. Although the minimum pitch ratio led to the highest exergy efficiency and friction factor increase by 173 % to 199 %, a ratio of 1.53 proved to have the greatest improvement in thermal-hydraulic factor [14]. These studies collectively indicate that while passive techniques effectively enhance heat transfer, they often introduce additional flow resistance, reinforcing the inherent trade-off between thermal performance and pressure drop. enhance the heat transfer rates by adding fluid dynamics and interaction characteristics based on the application of external energy sources, such as electric, magnetic, vibrating forces, and jet impingement. Although it is true that active methods provide additional factors that must be considered, design and operation complexities, and penalties regarding costs and maintenance, there are many potential advantages associated with their use as well [15–17]. Incorporating curved geometries, such as spirals and helical coils, continues to be one of the most effective passive techniques for improving heat transfer to date. The centrifugal forces produced by the curvature cause secondary vortex generation, thus leading to boundary layer disruption and increased Nusselt number [18]. Naphon (2011) conducted an experimental study on horizontal coil tubes and reported that performance is greatly enhanced through the use of spiral coil tubes relative to straight tubes, especially considering that the Nusselt number increases by 1.49 [19]. Zhang and Li (2014) conducted numerical research demonstrating that an increase in the eccentricity ratio of tube-in-tube helically coiled heat exchanger designs results in significant increases in the Nusselt number [20]. In the same context, the study conducted by Abdelmagied et al. (2024) investigated the thermo-fluid behavior of annular curved tubes using Al2O3–water nanofluids. Their numerical findings revealed that cross-sectional geometry plays a pivotal role in thermal performance, with the circular cross-section demonstrating superior heat transfer enhancement compared to elliptical, square, rectangular, and triangular shapes by 13 %, 30 %, 40.5 %, and 52.9**%** , respectively, for the same cross-sectional area [21]. In addition to such passive methods, incorporating rotational motion could result in further improvements. According to Sharma et al. (2024), the utilizing of controlled rotation on a helical tube with a porous medium can increase secondary flow, which can enhance the convective heat transfer in laminar and transitional region [22]. Although the Dean vortices (De) which is generated by centrifugal forces in coiled HXs have proved advantageous, and rotation of the tubes can result in increased heat transfer, such benefits cause a decay further downstream due to the breakdown of the Dean vortices, which form thermal “dead zones” and uneven temperature profiles along the coil [23]. Based on previous works, one can conclude that there are three categories of heat transfer enhancement processes, which include insert based, geometry alteration and active processes. Insert based processes such as twisted tapes or wire-coil inserts allows reaching high heat transfer enhancement efficiency, up to 68–111 % or even more; nevertheless, it has high pressure drop penalties caused by tube blockage and increased resistance. Geometry alterations like corrugated and spiral tubes offer medium levels of enhancement with pressure penalties, about 23–117 % for corrugated tubes and 30–80 % for spiral tubes. Rotating spiral tubes belong to active processes and enable even higher heat transfer efficiency, 145–160 %, but still, the pressure penalties are not extremely high. Therefore, despite the significant progress in heat transfer enhancement, a key challenge remains in achieving high thermal performance while maintaining low pressure-drop penalties and practical applicability.

In curved tubes, Dean vortices, which enhance radial mixing and disrupt the thermal boundary layer. However, these vortices gradually weaken along the flow direction due to viscous dissipation, reducing mixing intensity and heat transfer efficiency. In the present study, the introduction of periodic flow reversal segments is designed to locally reintroduce centrifugal effects, leading to the regeneration of Dean vortices. This mechanism enhances mixing, disrupts boundary layer development, and sustains convective heat transfer along the entire flow path.

A limitation of conventional horizontal spiral tubes is that curvature-induced secondary flow weakens downstream as viscous dissipation reduces vortex intensity. The proposed HSFR geometry addresses this limitation by introducing periodic 180° redirection of the internal flow, which locally regenerates secondary motion, renews near-wall mixing, and suppresses continuous thermal-boundary-layer growth. The objective of the present study is therefore to isolate and quantify the thermohydraulic effect of these integral flow-reversal segments relative to a conventional horizontal spiral tube under identical operating conditions. Considering the relatively low pressure-drop penalty of rotating spiral tubes [24], this study is motivated by combining tube rotation with flow reversal to further enhance heat transfer performance. An important technical merit of such a design is industrial ease of production, which allows reproduction by standard tube formation methods, unlike more specialized designs. Hence, such a design named Horizontal Spiral with Flow-Reversers (HSFR) is very amenable to modification and inclusion into a compact thermal system. In light of such a critical gap, the present work expands the work by Dabestani and Kahani (2024), which found optimal rotating characteristics of Horizontal Spiral Tube (HST) heat exchangers, to design, simulate, and critically assess an HSFR design with different Reynolds numbers [24]. In this work, HSFR is proposed, and its thermal-hydraulic behavior has been simulated by 3D CFD. The geometric parameters of the spiral tube, including pitch length, tube diameter, and number of turns, were selected based on previously validated configurations reported in [24]. The design was constrained to maintain equal heat transfer surface area between the HSFR and baseline HST configurations to ensure a fair performance comparison. The spacing and geometry of the flow reverser segments were determined to provide periodic flow redirection while keeping same surface area.

In Section 2, the computational methodology is described. Specifically, information is provided on the geometric shape and dimensions of the HSFR, the number and location of internal reversers, the description of rotating frame differential equations, the imposition of boundary conditions and temperatures, and the solution algorithms and models used by the Fluent R1 2025 solver. Moreover, a mesh-independence analysis is also discussed. In Section 3, validation of the numerical setup and comparison between the performances of HSFR and HST in various Re are conducted by investigating the velocity and temperature fields, and also by calculating Nu and Performance Evaluation Criteria, and Section 4 gives a discussion on the results obtained.

Nomenclature

Symbol / Acronym	Definition
HST	Horizontal Spiral Tube (conventional spiral tube heat exchanger)
HSFR	Horizontal Spiral Tube with Flow Reversers
HX	Heat Exchanger
CFD	Computational Fluid Dynamics
PEC	Performance Evaluation Criterion
Re	Reynolds number, $Re = \frac{\rho v D_i}{\mu}$
De	Dean number, $De = Re\sqrt{\frac{D_i}{D}}$
Nu	Nusselt number, $Nu = \frac{hD_i}{k}$
Gz	Graetz number, $Gz = \frac{\dot{m}C_p}{kD_i}$
Pr	
D_i	
D	
L	

(continued on next page)

(*continued*)

Nomenclature

Symbol / Acronym	Definition
ρ	Prandtl number, $Pr = \frac{C_p \mu}{k}$
μ	
V	Inner diameter of the tube
h	Curvature diameter of the coil
k	Tube length
c_p	Fluid density $[kg/m^3]$
$\vec{\omega}$	Dynamic viscosity $[Pa\cdots]$
τ	Fluid velocity $[m/s]$
Q	Convective heat transfer coefficient $[W/m^2.K]$
e	Thermal conductivity $[W/m.K]$
Φ	Specific heat capacity at constant pressure $[J/kgK]$
	Rotational angular velocity vector
$\lambda = \frac{D_{av}}{d}$	Viscous stress tensor
	Internal heat generation
$D_{av} = \frac{D+d}{2}$	Internal energy
$\vec{v}_r$	Dissipation function
$\vec{v}$	Curvature ratio
$\vec{F}$	Average diameter of spiral coil
$\nabla .$	Relative velocity
$\dot{m}$	Absolute velocity
$\vec{r}$	Force term
	Divergence
$\Delta P = f\frac{L}{d}\frac{\rho v^2}{2}$	mass flow rate
f	Position vector
	Pressure drop
	Friction factor

2. Simulation details

2.1. Geometry and model construction

In regard to the computational-geometry work conducted within the scope of this research, it should be noted that it has been developed utilizing the Autodesk Inventor 2025 and is illustrated in Fig. 1. In turn, it comprises an external shell and an internal horizontal spiral tube, which features the HSFR design. In the HSFR, periodic 180-degree fluid path turnings are imposed. Table 1 shows the geometric details of the components of the heat exchanger in both HST and HSFR cases, which indicate the design criteria. These design criteria were used to ensure maximum efficiency and manufacturability, which are supported by the designs cited by Dabestani and Kahani [24]. The design of the total heat transfer surface areas of the HSFR and the HST base configurations were made equal. This is essential to ensure that the performance improvements, if any, are due to the geometrical changes.

Table 1
Geometric Design Parameters for Spiral Tube Heat Exchanger.

Parameter	Value (HSFR)	Value (HST)	Unit
Shell Diameter	600	600	mm
Shell Height	200	200	mm
Tube Diameter	10	10	mm
Tube Length	2700	3100	mm
Coil Outer Diameter	368	340	mm
Coil Inner Diameter	47	60	mm
Pitch Length	23	23	mm
Number of Turns	5	5	

2.2. Boundary layer characteristics

The solution domain is divided into two regions: the first domain involves the inner tube, which is described by a rotating reference frame centered on the tube Z-axis, and the second domain involves the remaining surrounding shell, which is stationary. The tube rotates counterclockwise, and the rotation vector points along the Z-axis, following the right-hand rule. Table 2 describes the essential parameters influencing the evolution of the boundary layer.

Table 2
Boundary Conditions for Shell and Tube Heat Exchanger Simulation.

Parameter	Type	Value	Unit
Tube Inlet	Velocity Inlet	0.09–0.28	m/s
Tube Inlet	Temperature	333	K
Tube Outlet	Pressure Outlet	0	Pa
Shell Inlet	Velocity Inlet	0.15	m/s
Shell Inlet	Temperature	293	K
Shell Outlet	Pressure Outlet	0	Pa
Walls	No-slip Boundary Condition		
Tube Inner and Outer Wall	Coupled		
Shell External Wall	Adiabatic		
Spiral Tube	Rrotating Frame	4	RPM

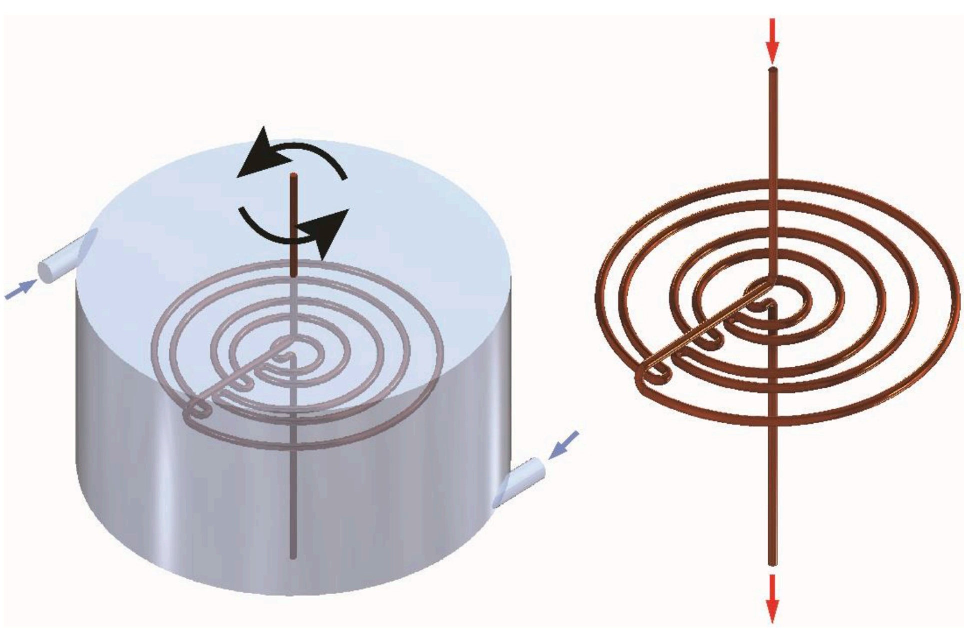

Fig. 1. Geometric configuration of the spiral heat exchanger with internal flow reversers (HSFR).

2.3. Material properties

In the present work, water is used as the fluid owing to its applicability to heat transfer systems. Water is assumed to behave as a Newtonian, incompressible fluid, which is true under the operational conditions. Moreover, fluid properties such as density, viscosity, specific heat, and thermal conductivity are assumed to vary with temperature. The spiral tube and shell are made of copper, which has high thermal conductivity and easy workability. Heat transfer between the tube-side hot fluid and the shell-side cold fluid was modeled using a conjugate heat transfer approach through the tube wall. The wall itself is represented as a coupled interface boundary between the solid wall and the neighboring fluid zones. The heat transfer across the wall will be calculated depending on the temperature distribution in the neighboring cells.

In order to keep the problem physically correct but numerically simplified, the following approximations were used: Steady state, three-dimensional, incompressible flow. Newtonian fluid (water). Effects of radiation heat transfer are not taken into account. No heat losses to the environment, heat exchange takes place only between the two fluid streams.

2.4. D. governing equations and numerical procedure

The thermal and hydrodynamic performances of the HSFR were numerically simulated using the commercial software, ANSYS Fluent 2025 R1. The simulations were based on the conservation equations of mass, momentum, and energy. They were simulated using a rotating frame of reference to correctly capture the influences of tube rotation and curvature. The additional source terms, due to rotation and tube curvature, were used to add the influences of centrifugal and Coriolis forces to the equation. These forces cause secondary currents, also known as Dean vortices, which increase the radial mixing and convective transport [25]. This modeling approach follows the methodology established by Tey et al., which enables accurate prediction of complex flow phenomena within the HSFR geometry Tey et al [26]. The governing equations are given by:

Continuity Equation:

$$\nabla.\left(\rho\vec{v}_r\right) = 0 \tag{1}$$

Momentum Equation (Navier–Stokes in Rotating Frame):

$$\nabla.\left(\rho\left(\vec{v}_r\vec{v}_r\right) + 2\rho\left(\vec{\omega}\times\vec{v}_r\right) + \rho(\vec{\omega}\times(\vec{\omega}\times\vec{r})) = -\nabla p + \nabla.\tau + \vec{F}\right. \tag{2}$$

Energy Equation:

$$\nabla.\left(\rho\vec{v}_r C_p T\right) = \nabla.(k\nabla T) \tag{3}$$

Where $\vec{v}_r$ represents the velocity relative to the rotating reference frame, $\vec{v}$ denotes the absolute velocity in the stationary frame, and $\vec{\omega}$ is the angular velocity vector describing the rotation of the spiral tube. The fluid velocities can be transformed from the stationary frame to the rotating frame using the relation:

$$\vec{v}_r = \vec{v} - \vec{\omega}\times\vec{r} \tag{4}$$

where $\vec{r}$ is the position vector from the rotation axis to a point in the fluid.

$2\left(\vec{\omega}\times\vec{v}_r\right)$ represents the Coriolis acceleration. And $\vec{\omega}\times(\vec{\omega}\times\vec{r})$ represents the Centripetal acceleration.

To focus on laminar flow characteristics and isolate enhancement mechanisms independent of turbulence, the Reynolds numbers were restricted to lower than the critical value. Although transition happens around 2300 in the case of a straight pipe, the effect of curvature enhances the same because of stabilization secondary flows. Correlation 5 for critical Reynolds number in coiled pipes was applied to obtain the critical Reynolds number [27]:

$$Re_{Cr} = 30000/\lambda^{0.47} \tag{5}$$

To focus on laminar-to-transitional curved-pipe behavior and avoid fully turbulent conditions, the Reynolds number was limited below $Re =$ 6300. The SST k–ω model was employed to ensure robust prediction across this regime.

2.5. Solver settings

The SIMPLE algorithm was used to couple the velocity and pressure due to its suitability to handle problems involving incompressible fluid flows and its balance of computational efficiency and solution accuracy [28]. A second-order upwind scheme was used to discretize the momentum and energy equations. This provided higher accuracy than first-order methods [29].

2.6. Meshing strategy

A structured hexahedral mesh was generated by ANSYS Fluent Meshing for the computational domain. The choice of the type of mesh is crucial for the simulation of internal flows. A hexahedral mesh was selected for the computational domain because of its better robustness and higher accuracy compared to other types of meshes in modeling near-wall effects [30]. Although the Reynolds number range (2000–6000) lies within the laminar-to-transitional regime for curved pipes, the flow in the present configuration is continuously disturbed due to curvature, rotation, and periodic flow reversal. These effects promote local instabilities and transition-like behavior. Therefore, the SST k–ω turbulence model was employed to ensure accurate prediction of near-wall gradients and to capture possible transitional effects. The SST k–ω model is well known for its robustness in handling adverse pressure gradients and complex flow separation. To ensure near-wall accuracy, the mesh was refined such that $y^+ < 1$ throughout the domain, and the flow was fully resolved without the use of wall functions. Inflation layers with a growth rate of 1.2 were utilized along the surface of the tube walls in order to account for the near-wall gradients. A total number of five inflation layers was used for a first layer thickness of about 0.3 mm. No wall functions were used since the present study had laminar and transitional flow regimes. Therefore, the equations were solved directly to the wall. Further mesh refinement was done in areas of high gradients; particularly at the reverser bends and inlet/outlet regions. Fig. 2 below shows the mesh configuration. A similar meshing strategy was applied to both geometries to ensure consistency in comparison.

In order to verify the correctness and accuracy of the obtained numerical solution, a mesh independence study has been carried out. The aim of this, is to reveal the most optimal mesh density, which should accurately reproduce the system's thermal regime without increasing the complexity of computations unnecessarily. The Nu and ΔP has been used to assess the performance of various mesh sizes. The number of elements between 650,000 and 2000,000 was generated and tested under identical operating conditions. As shown in Fig. 3, the Nusselt number increases with mesh refinement and gradually approaches an asymptotic value. When the number of elements increases beyond approximately 1.4×10^6, the variation is insignificant. The quantitative results of the grid independence analysis are summarized in Table 3. Specifically, the difference in Nu between the meshes with 1.45×10^6 and 1.2×10^6 elements is <0.5 %, also the corresponding variation in pressure drop is 1.16 %. These results show that both thermal and hydraulic predictions are mesh-independent. Therefore, a mesh with

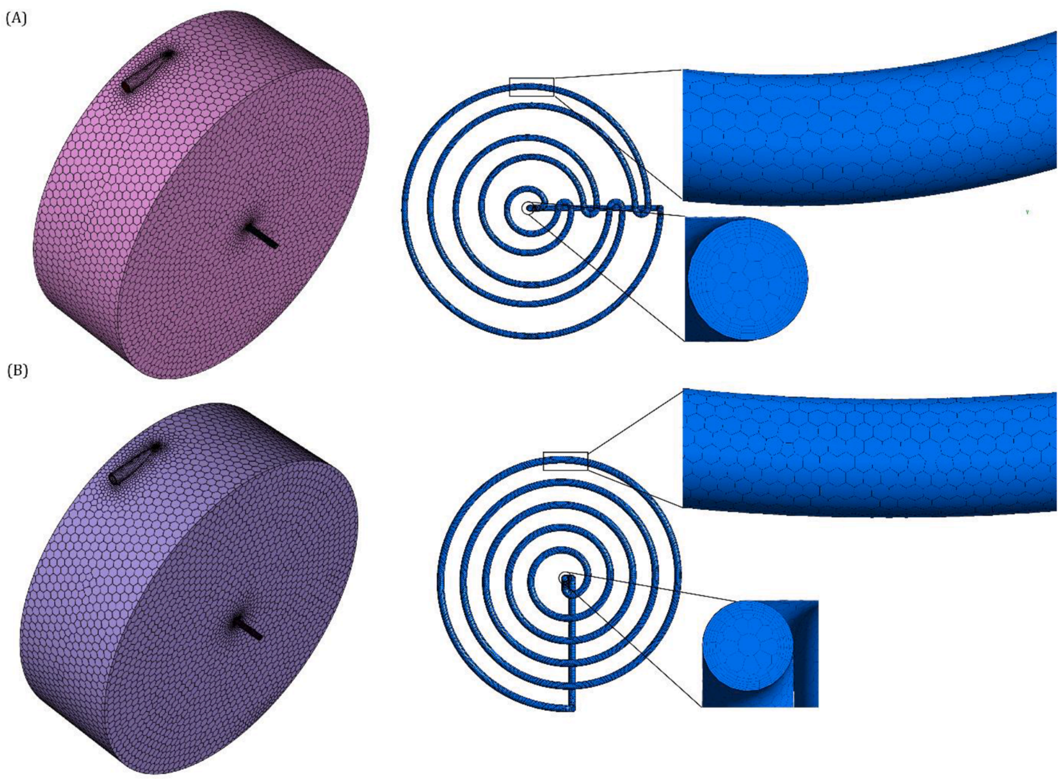

Fig. 2. Mesh representation of the computational domain with close-up around the spiral tube, (A) HSFR (B)HST.

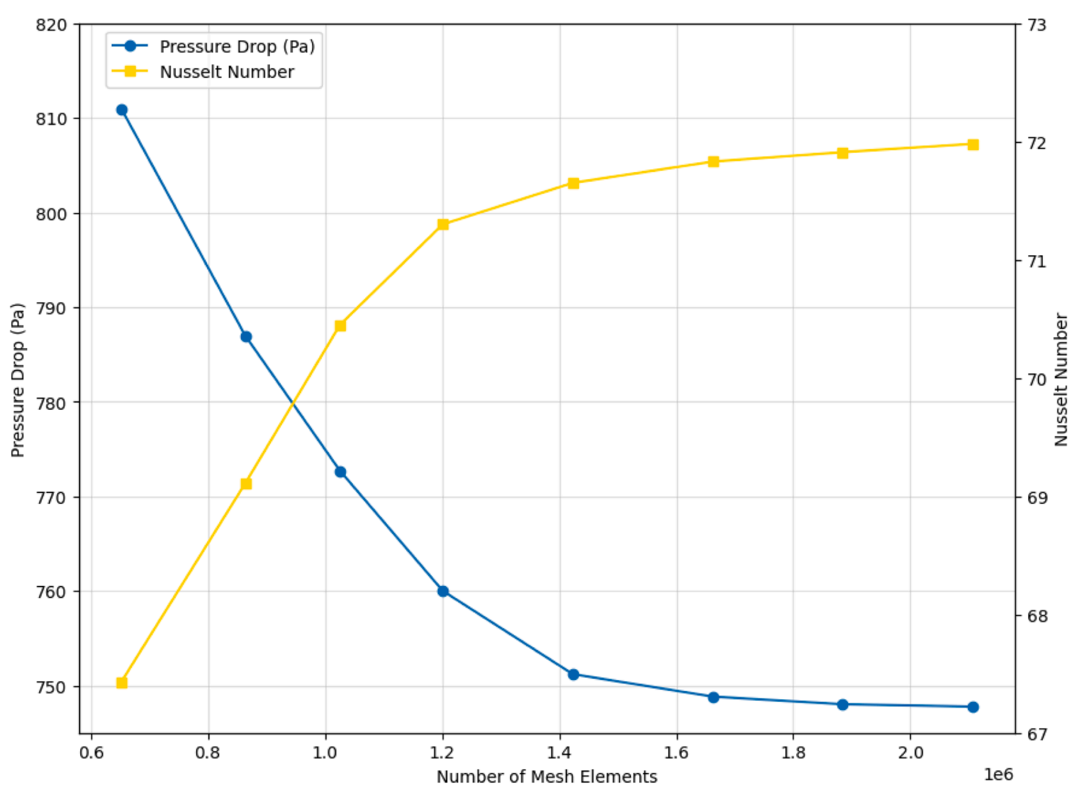

Fig. 3. The Nu number and pressure drop in the coil side for different numbers of grids.

approximately 1.42 $\times$ 10^6 elements was selected for all subsequent simulations as a compromise between computational cost and numerical accuracy.

The grid independence study was further quantified using the Grid Convergence Index (GCI) method. Three successively refined meshes with 1025,873, 1201,457, and 1423,497 elements have been used for

Table 3
Quantitative grid independence results.

Elements	Nu	Relative Error	ΔP	Relative Error
652,340	67.43	—	810.97	—
864,125	69.11	2.49 %	786.89	2.96 %
1,025,873	70.45	1.94 %	772.69	1.82 %
1,201,457	71.30	1.21 %	760.00	1.64 %
1,423,497	71.65	0.49 %	751.20	1.16 %
1,662,101	71.83	0.25 %	748.83	0.32 %
1,884,510	71.91	0.11 %	748.02	0.11 %
2,105,328	71.98	0.10 %	747.77	0.03 %

the calculation of the GCI. As per the findings from Nu, the fine-grid GCI value was found to be equal to 1.81 %, indicating low discretization uncertainty. For the ΔP, the corresponding fine-grid GCI was approximately 5.43 %, reflecting the higher sensitivity of hydraulic predictions to mesh resolution. Nevertheless, both the Nu and ΔP showed monotonic behavior for decreasing relative difference with increasing number of grid cells, becoming negligible after approximately 1.4×10^6elements. Therefore, the mesh with 1423,497 elements was selected for all subsequent simulations.

3. Results and discussion

3.1. Validation

In a validation analysis, the accuracy of the computational models has been tested by correlating the calculated Nu with various study results including published correlations and experimental-based equations. The calculated process has been viewed under the conditions of a shell and a static horizontal spiral tube heat exchanger, with various ranges of the Reynolds number (*Re*). The calculated result has been verified with various results provided by Etghani and Baboli [31], Jayakumar et al. [32], Patil et al. [33]. As shown in Fig. 4, the present numerical results are in good agreement with the experimental-based correlation [33]. The deviation between the numerical prediction and the experimental data is <13 %.

Further simulations were carried out to explore the effect of rotational motion on convective heat transfer in a HST configuration. The obtained Nu were verified against the information provided by Dabestani and Kahani [24]. Fig. 5 shows how the simulated model is in good agreement with the reference values. Such an agreement strengthens the robustness of the computational method and provides the basis for its application in the HSFR design of the current work.

3.2. Flow pattern

Fig. 6 the velocity distribution on the tube side and in the same cross-section of the last turn of the spiral tube with the presence of the flow reverser under the operating conditions (*Re* 2000, 4000 and 6000; ω=4 RPM). The presence of the flow reverser causes a considerable change in the behavior of the fluid flow. In the HST case, it is noticed that the velocity distribution has a strong peak along the axis with high gradients near the tube wall, which causes strong shear layers and asymmetric secondary flows, associated with strong changes in fluid flow distribution. In contrast, the HSFR case has a more homogeneously distributed velocity profile along the axis, with lower gradients and a more uniform distribution across the section. The modification of the velocity field is mainly attributed to the regeneration of the Dean vortices created by the flow reverser segments. Due to the periodic 180-degree deflection of flow in the HSFR geometry, local re-introduction of centrifugal force results in the development of additional secondary vortices, which help enhance the lateral transfer of momentum and increase radial velocities, thus promoting mixing and preventing the development of stagnant or low-velocity regions within the tube. Fig. 7 illustrates the velocity distribution inside the shell domain for two spiral heat exchangers. The shell-side and tube-side conditions were kept identical for the evaluation. The effect of the internal tube configuration on shell-side flows is considerable. As shown in Fig. 8, in the case of the HSFR, periodic internal flow reversers are used, which disturb the internal fluid motion by reducing the axial component and increasing the radial component of the momenta. These disturbances propagate through the tube wall and affect the adjacent shell fluid, resulting in pronounced asymmetries and irregularities in the velocity field. This process enhances mixing in the shell side, increasing heat transfer by promoting more contact of the fluid with the outer tube surface. The intensified mixing underlines the

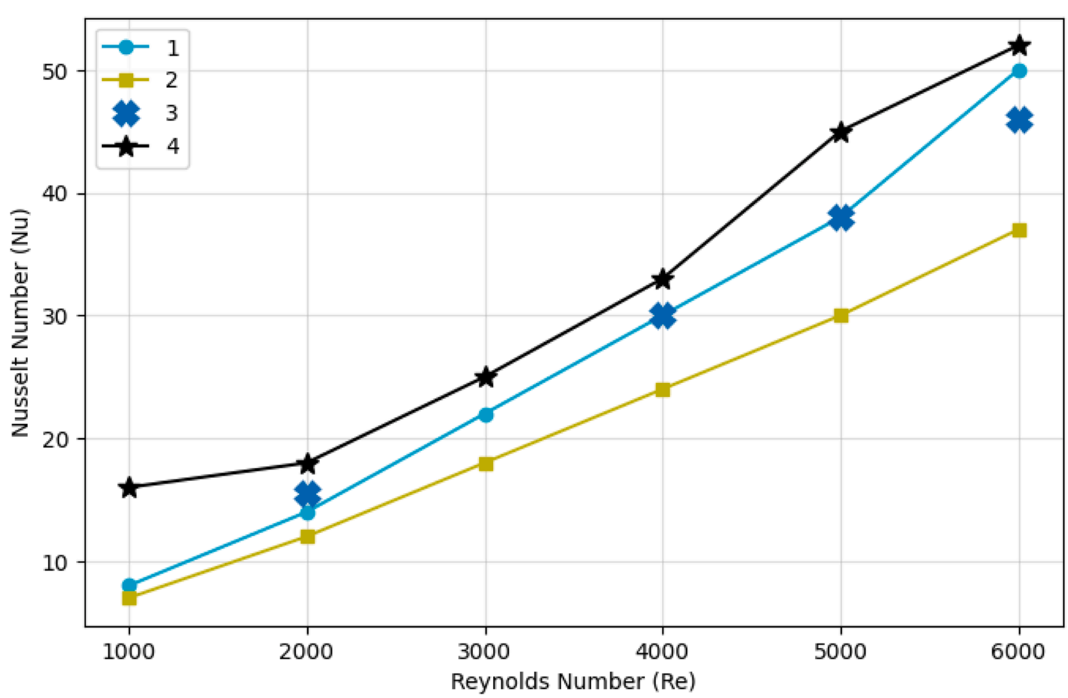

Fig. 4. Comparison of Nu from correlations by 1: Etghani & Baboli [31], 2: Jayakumar et al. [32], 3: CFD, and 4: Pati et al. [33].

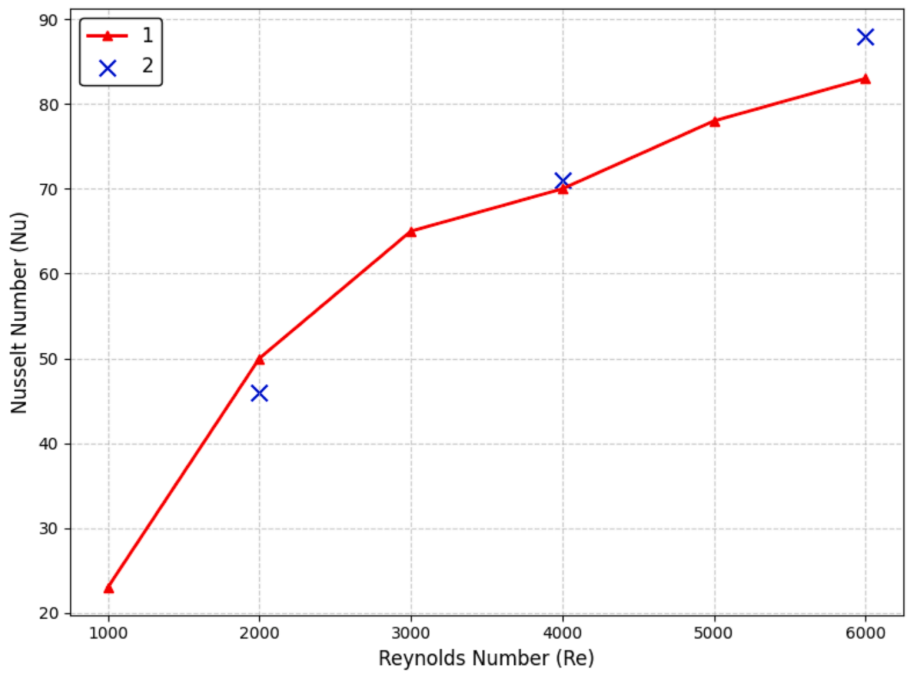

Fig. 5. Validation of Nu for this study (2) against $\omega = 4$ RPM from Dabestani et al. [24] (1).

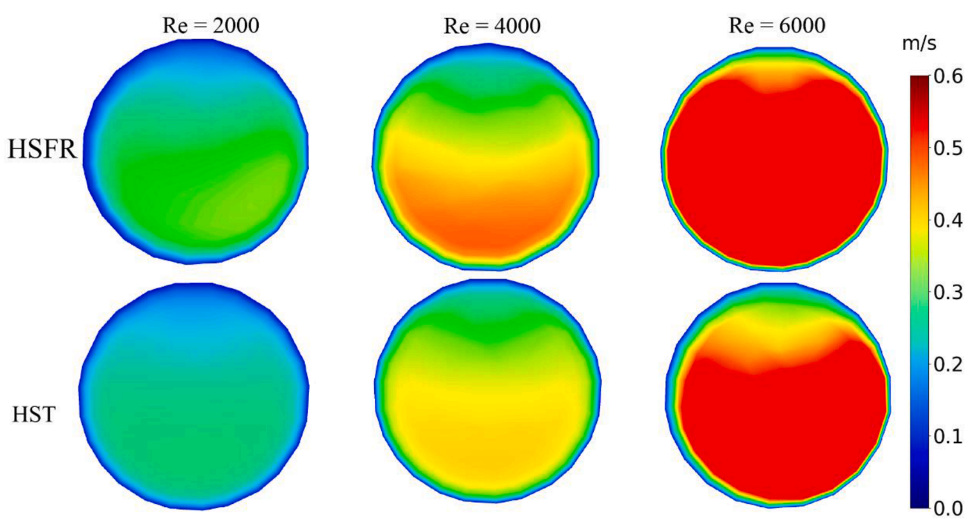

Fig. 6. Cross-sectional velocity profile for HSFR and HST at different Reynolds numbers under $\omega = 4$ RPM rotation.

ability of the HSFR design to enhance the heat transfer process outside the tube region, further enhancing the efficiency of the overall system. In comparison, the heat exchanger with HST maintains a flow pattern that is steadier, resulting in a symmetrical and layered velocity field with minimal mixing. This uniformity can dampen thermal performance because it reduces how much the fluid interacts. An important benefit of the HSFR design, which is distinct and unique to other passive internal insert designs, is the strong influence on the shell-side flow field.

Fig. 9 shows the flow structures for the cross-section of the last turn of flow passage for both HSFR and HST configurations. In the HST case, the secondary flows generated are quite weak and have relatively uniform distribution without any cross-sectional movement, meaning that there is less mixing and the development of thermal boundary layer will occur along the wall of the tube. On the other hand, the secondary flows formed in the HSFR geometry are much stronger because of the flow reversers used, and therefore there are repeated deflections of the flow and creation of recirculating vortices and cross-sectional flow.

3.3. *Temperature profile*

Fig. 10 shows the fluid temperatures inside the spiral tube at various cross-sections for HST and HSFR arrangements at $Re = 2000$, 4000, and 6000. The maps of temperatures demonstrate how much the working fluid is cooled by the heat transfer. The difference between HST and HSFR designs shows the latter has a greater temperature difference, which reflects greater heat transfer to the tube wall and then to the ambient surroundings. Fig. 11 also displays the corresponding temperatures on the shell side. In the case of the HSFR design, the heated region surrounding the tube is wider and has more gradual temperatures, signifying an efficient transfer of fluid temperatures to the tube and the surrounding shell fluid. The increased fluid turbulence inside the tube due to the installed reversers causes a more efficient transfer of the heat to the shell. In contrast, the HST design has a localized heated zone with steeper temperatures near the tube, which reduces the transfer of fluid temperatures to the shell. As a result, the presence of flow reversers

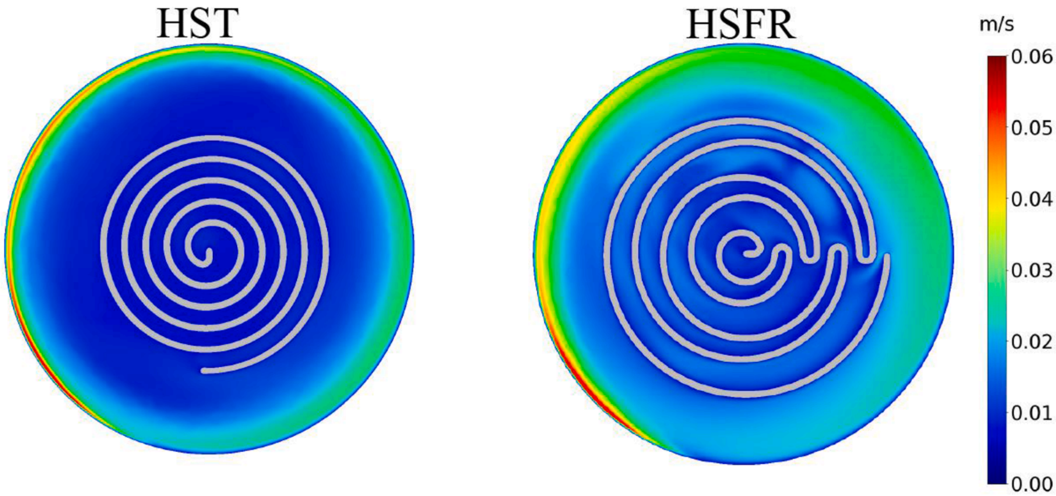

Fig. 7. Shell-side velocity profile for horizontal spiral tube heat exchangers with HSFR and HST at Re=6000.

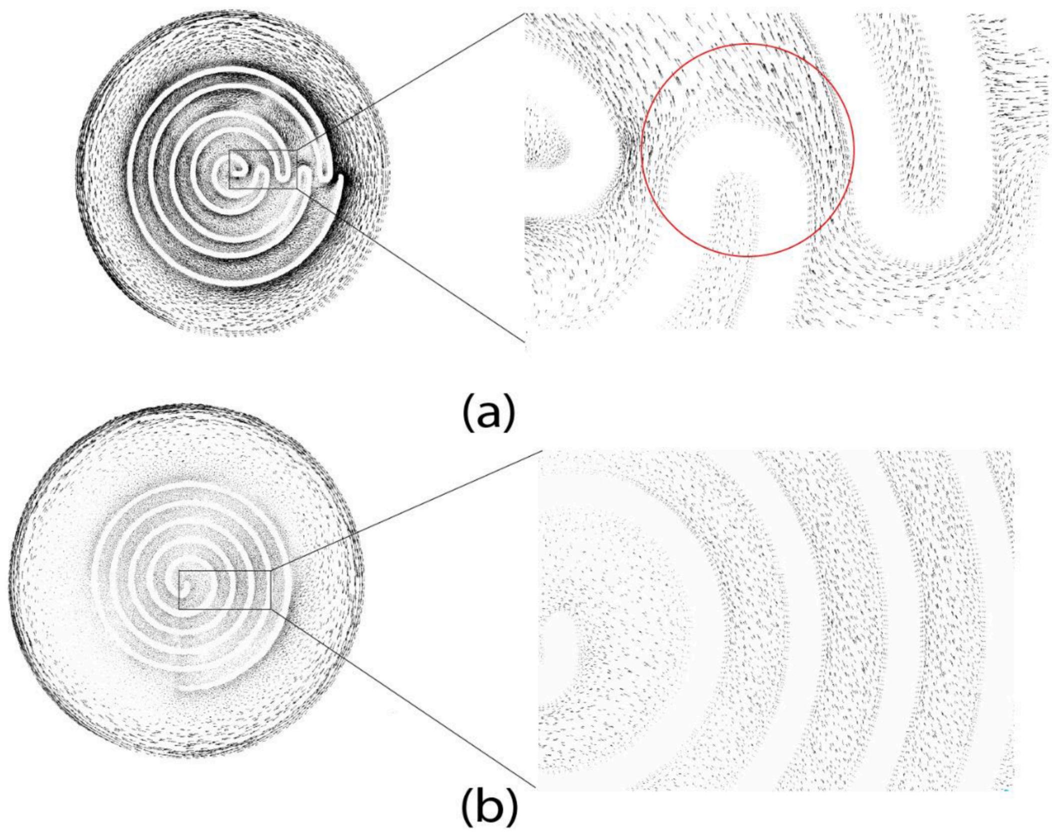

Fig. 8. Velocity vectors in the shell region: (a) HSFR and (b) HST.

significantly improves the efficiency of spiral tube heat exchangers. As shown in Fig. 12 that the average Nusselt number increases with Reynolds number for both configurations, but its variation for HSFR is consistently greater than that for HST. The fact suggests that the improved heat transfer by HSFR is due to the effect from flow modification. In the HST design, the induced secondary flow becomes increasingly weaker towards the exit point of the spiral, resulting in an increased thickness of the thermal boundary layer and limiting the potential enhancement in the wall heat flux. On the other hand, the reversers in HSFR continually modify the velocity distribution and regenerate the cross-flow, which facilitates the transport of heat flow across the tube centerline. With the increasing Reynolds number, the inertia and centrifugal force become significant, so each reversal produces a larger disturbance of the developing thermal boundary layer; this explains why the relative HSFR advantage grows with Reynolds number. Compared to HST, it is found that Nu increases under the HSFR configuration by 16.3 %, 26.8 %, and 32.9 %, corresponding to Re of 2000, 4000, and 6000, respectively. Thus, it is verified that the new design is more advantageous than HST.

The observed enhancement in Nusselt number for the HSFR configuration is primarily attributed to intensified fluid mixing and repeated disruption of the thermal boundary layer. The repeated flow redirection prevents the continuous growth of the thermal boundary layer along the flow direction, maintaining a thinner boundary layer thickness. This

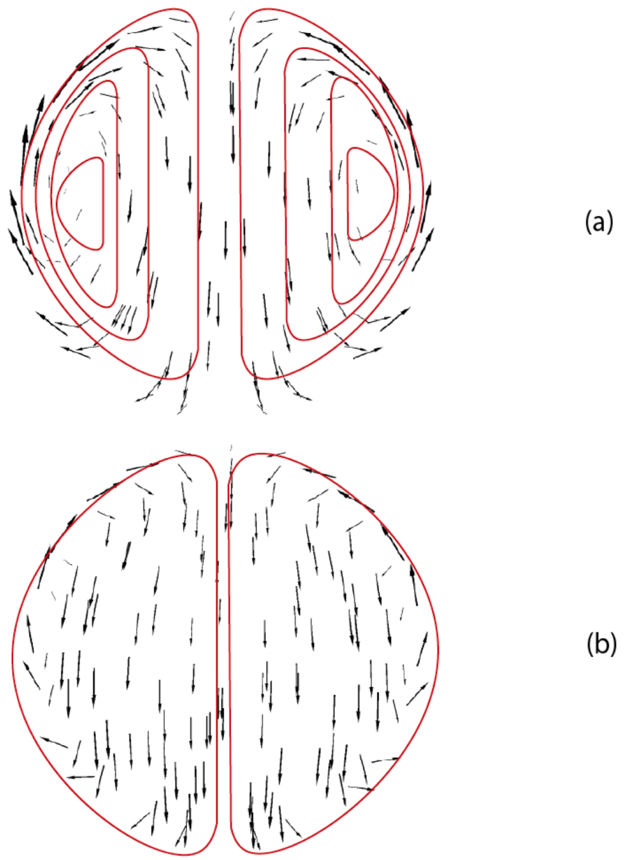

Fig. 9. Secondary flow structures in the cross-section of the last turn for (a) HSFR and (b) HST.

results in higher temperature gradients at the wall and consequently increased convective heat transfer.

3.4. Pressure drop

The pressure drop characteristic is an essential part of the performance evaluation process, besides thermal efficiency, and is critical when examining the compromise between increased heat transfer and increased pumping work. In Fig. 13a comparison between the pressure drop of HST and HSFR is offered over a range of *Re* between 2000 and 6000. In the low-*Re* regime, it is difficult to differentiate between the pressure drop of HST and HSFR, and a negligible difference between the pressure drop of the HST and HSFR systems suggests that, at low *Re*, the insertion of reversers has resulted in merely a minor increase to the hydraulic losses. As *Re* increases, the pressure drop difference becomes more distinct. This is due to flow reversers interfere more substantially with fluid momentum, which generates additional recirculation zones.

To evaluate the performance of HSFR when compared to the HST, the performance evaluation criteria (PEC), which is defined by Webb [34], has been calculated based on the following expression:

$$PEC = \frac{\frac{Nu_{HSFR}}{Nu_{HST}}}{\left(\frac{f_{HSFR}}{f_{HST}}\right)^{\frac{1}{3}}} \tag{6}$$

This criterion translates the compromise between the benefits of increased heat transfer and the corresponding pressure drop. A PEC value greater than 1 indicates that it is advantageous to employ the design, which is more efficient. Fig. 14 The increase of PEC from approximately 1.11 at $Re = 2000$ to 1.27 at $Re = 6000$ confirms that the HSFR enhancement mechanism becomes more favorable as the flow inertia increases. This trend is important because it shows that the added pressure drop does not scale as severely as the heat-transfer benefit.

3.5. Dimensionless correlations

In order to extrapolate the numerical values and provide an engineering tool, dimensionless correlation for Nu and friction factor (f) was obtained for both the HST and HSFR geometries. These correlations consider the effects of curvature, rotation, and flow reversal within each curve at 4 RPM, and over the Reynolds numbers studied between 2000 and 6000. The form of the correlations follows the traditional power law form Table 4:

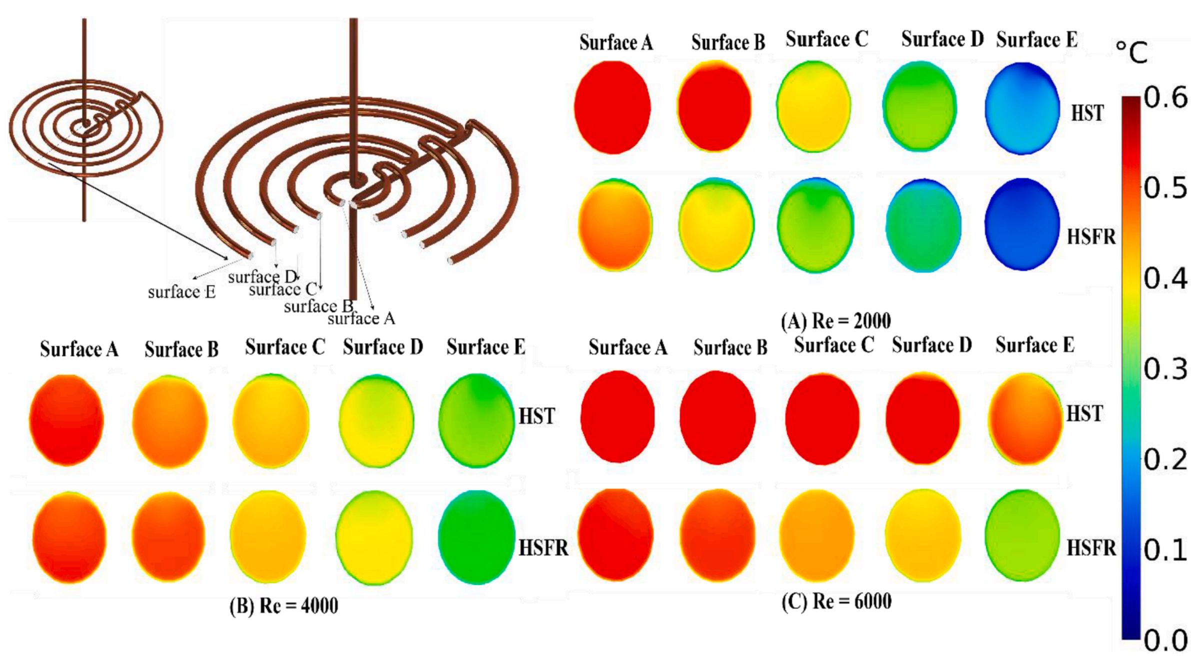

Fig. 10. Temperature profile along the spiral tube for HSFR and HST in various Reynolds numbers.

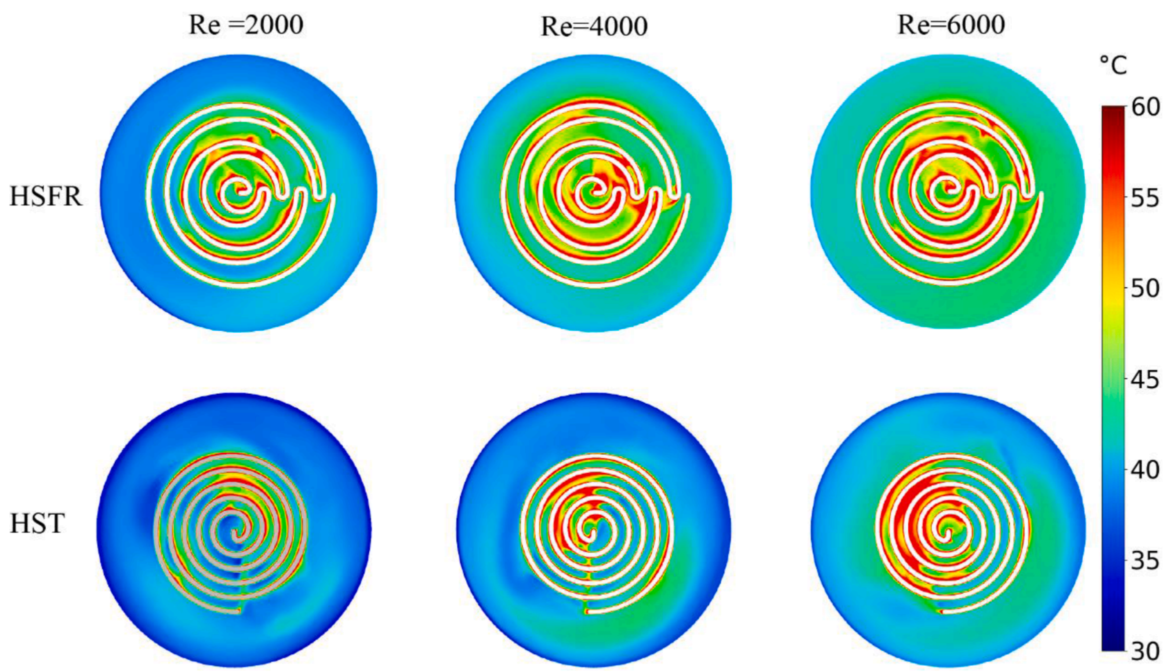

Fig. 11. Shell-side thermal fields for HST and HSFR configurations under varying Reynolds numbers.

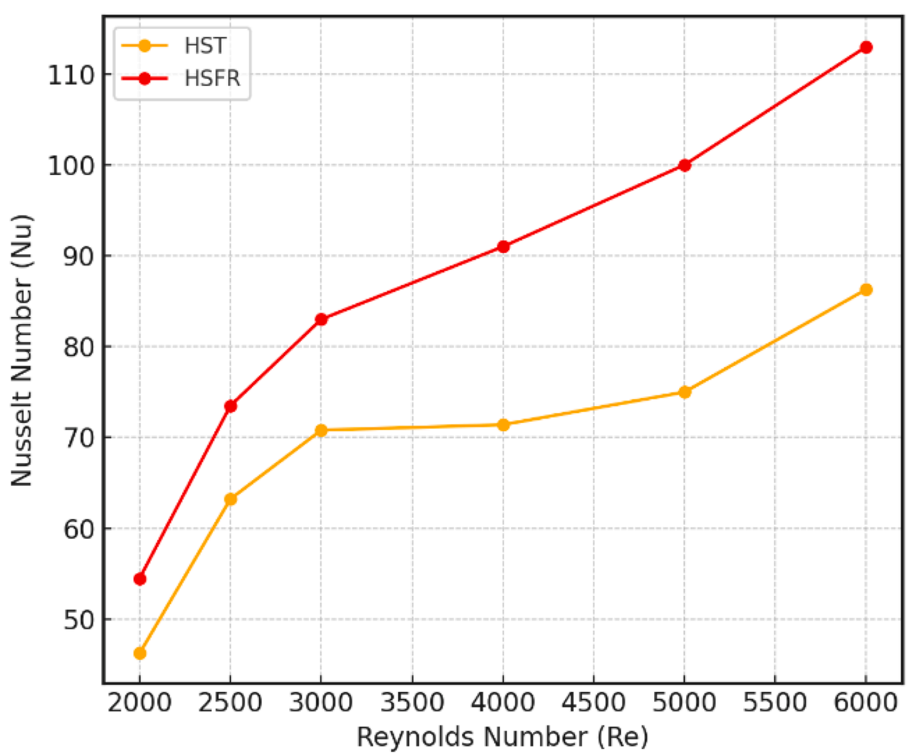

Fig. 12. Tube side Nusselt number versus Reynolds number for HST and HSFR configurations.

4. Conclusion

This study addressed a key limitation of conventional horizontal helical spiral tubes, namely the downstream weakening of curvature-induced secondary flow and the associated growth of the thermal boundary layer, resulting in reduced heat transfer effectiveness along the flow path. In order to overcome this weakness, a helical spiral tube with flow reversers (HSFR) was proposed and compared against the classical configuration of the helical spiral tube (HST) using 3D numerical simulations. The innovative aspect of the current work is in the employment of periodic flow reversal to locally generate Dean vortices without utilizing any internal structures and causing more pressure drop.

Under the investigated operating conditions, corresponding to Reynolds numbers of 2000–6000, three-dimensional steady incompressible conjugate heat transfer, water as the working fluid, a rotating-frame

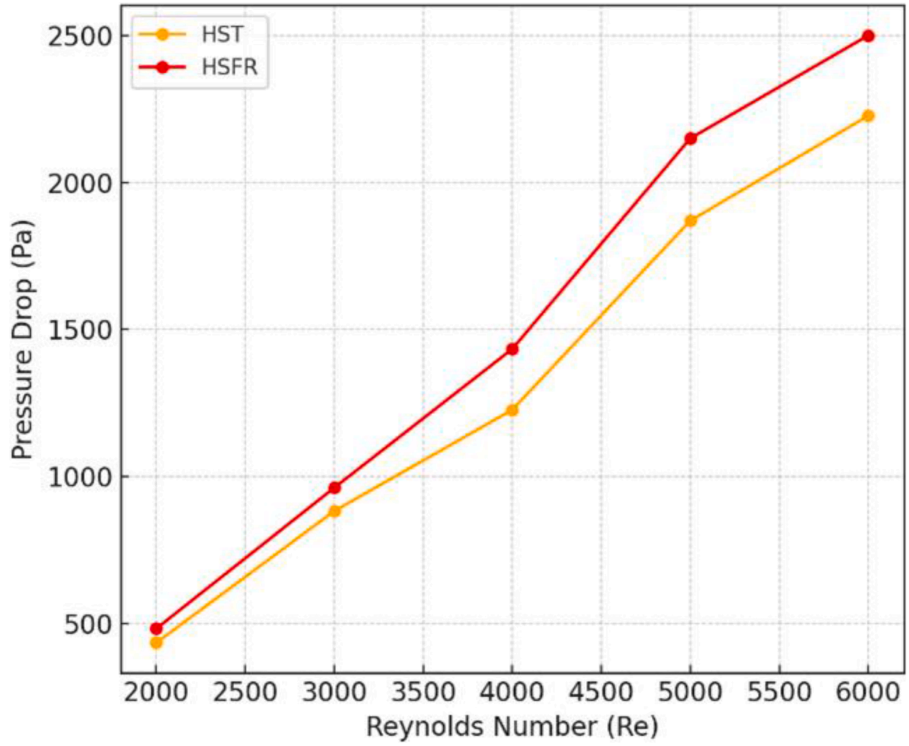

Fig. 13. Pressure drop variation for HST and HSFR configurations across Reynolds numbers.

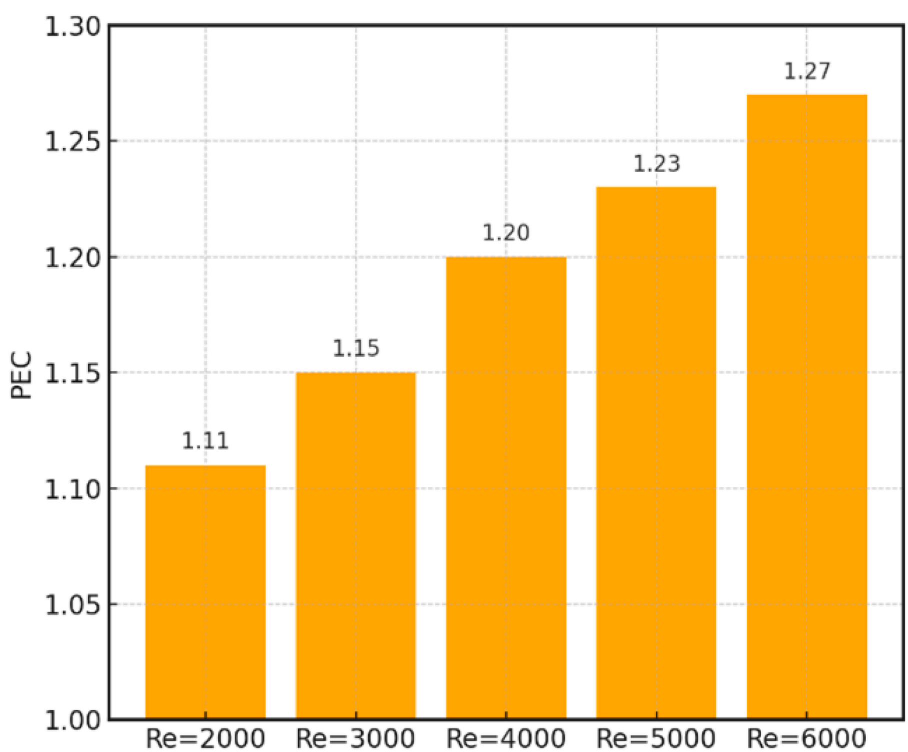

Fig. 14. Performance Evaluation Criterion (PEC) values for HSFR compared to HST at different Reynolds numbers.

formulation. Relative to the HST, the HSFR increased the tube-side Nusselt number by 16.3 %, 26.8 %, and 32.9 % at Reynolds numbers of 2000, 4000, and 6000, respectively, while the corresponding pressure-drop penalty remained moderate at 6.7 %, 17.9 %, and 12.6 %. The thermohydraulic benefit was therefore favorable over the entire investigated range, with the performance evaluation criterion remaining greater than unity and reaching 1.27 at $Re = 6000$.

The improvement in thermohydraulic performance comes from converting the usual vortex decay inherent in a conventional spiral tube to an intermittently regenerated transport phenomenon. Each reverser modifies the local velocity field, generates recirculation, and causes reattachment, and also provides for renewing near-wall fluid motion

Table 4
Dimensionless correlations for thermal and hydraulic performance.

Configuration	Nu correlation	Friction factor (f) correlation	R^2
HST	$Nu = 0.415Re^{0.573}.Pr^{1/3}$	$f = 11.21Re^{-0.582}$	0.988
HSFR	$Nu = 0.529Re^{0.576}.Pr^{1/3}$	$f = 12.56Re^{-0.585}$	0.992

while maintaining the wall-normal temperature gradient. Hence, the local wall heat flux increases, which leads to a substantial rise in the Nusselt number. These structures generate additional hydraulic resistance losses; however, the pressure drop increase is still less than the increase in heat transfer, as confirmed by PEC > 1. The performance enhancement of the HSFR design can be attributed to three key mechanisms: (1) regeneration of Dean vortices via repeated changes of the direction of flow motion, (2) increased mixing owing to higher radial velocity gradients, and (3) disruption of the thermal boundary layer. These combined effects lead to sustained heat transfer enhancement along the entire flow path, in contrast to conventional spiral tubes where vortex decay reduces thermal performance downstream. As shown in Table 5, conventional enhancement techniques such as twisted tapes, wire-coil inserts, and corrugated tubes can achieve high heat transfer enhancement (typically 68–111 % and up to 117 % or higher). However, these methods are associated with substantial pressure-drop penalties, often in the range of 3–4 times that of a plain tube, due to internal blockage and increased flow resistance.

In contrast, spiral tubes provide moderate enhancement (30–80 %) with lower pressure penalties (1.5–3 ×), but their performance is limited by the decay of secondary flow structures along the flow path. Rotating spiral tubes further improve heat transfer (145–160 %) with only a modest increase in pressure drop (~1.13 ×). The proposed HSFR configuration combines the advantages of geometric enhancement and flow reorganization, achieving a significant overall heat transfer enhancement of approximately 187–221 % while maintaining a relatively low pressure-drop penalty (1.2–1.4 ×). Unlike insert-based methods, the HSFR design does not introduce internal obstructions, reducing fouling risk and simplifying maintenance. Therefore, it offers more favorable thermohydraulic performance and practical applicability compared to conventional enhancement techniques.

5. Industrial significance

The HSFR configuration offers various distinct advantages for use in an industry, particularly concerning the reduction of equipment size, lower energy use, and ease of operation. In the context of an industry, the HSFR can easily be manufactured by common tube-forming, mandrel bending, and even the process of extrusion, as commonly applied to shell and tube heat exchanger design. In addition, the HSFR does not face Fouling, vibration, metal fatigue, and insert blockage, which are common problems experienced by other inserts such as the twisted tape, wire coil, and internal vortex generator, which are often installed, anchored, and later removed during maintenance.

Operationally, the HSFR design provides the capability for increasing the heat transfer per unit area. This becomes particularly important for desalination plants, pharmaceutical processing, the food industry, chemical reactors, and waste heat recovery applications, where space and cost considerations are important factors. The generation of perturbation along the length of the tube provides an important means for the control and stability of the process. Energy use is another major consideration in industry. The HSFR supports up to 32.9 % higher Nusselt number for equal flow rates, involving only a small penalty for the total pressure drop, thus ensuring improved thermohydraulic performance as compared to the conventional horizontal spiral coil. As such, either (1) the same heat transfer task can be accomplished using less pumping power, or (2) the same amount of pumping power can produce an enhanced heat transfer, which reduces the cost of operation.

Finally, the fact that the system does not contain moving parts inside the flow passage, makes the HSFR system robust and, therefore, amenable to industry-ready retrofitting and incorporation into future generations of compact heat exchangers. In aggregate, it appears that the various advantages discussed are sufficiently indicative of the fact that the HSFR has the potential to be far more than just an effective research tool.

Table 5
Comparison of enhancement techniques with the proposed HSFR configuration.

Method	Typical heat transfer enhancement	Pressure-drop penalty	Practical limitation
Twisted tapes [11]	68–99 %	3.46–4.12 ×	High friction, internal blockage
Wire–coil insert [35]	85–111 %	3.5 ×	High friction, internal obstruction
Corrugated tube [36]	23–117 %	3–3.5 ×	Manufacturing complexity, High friction
Spiral tube [37]	30–80 %	1.5–3 ×	
Rotating spiral (compared with spiral tube) [24]	145–160 %	1.13 ×	
Rotating spiral reverser (compared with spiral tube)	187–221 %	1.2–1.4 ×	

6. Future work

While the present study provides a numerical investigation of the thermohydraulic performance of the HSFR configuration, a systematic parametric study of geometric variables, including pitch, curvature ratio, flow reverser spacing, and blockage ratio, is recommended. Although these parameters were intentionally kept constant in the current work to isolate the effect of flow reversal, their optimization could lead to further enhancement of heat transfer performance and improved thermohydraulic efficiency.

Declaration of generative AI and AI-assisted technologies in the manuscript preparation process

During the preparation of this work the authors used ChatGPT to correct grammatical errors and improve the manuscript. After using this tool, the authors reviewed and edited the content as needed and took full responsibility for the content of the published article.

CRediT authorship contribution statement

Mohammad Mobin Bakhshi: Writing – original draft, Visualization, Validation, Software, Resources, Project administration, Methodology, Investigation, Funding acquisition, Formal analysis, Data curation, Conceptualization. **Faezeh Ahangar:** Writing – original draft, Visualization, Validation, Software, Methodology, Formal analysis, Data curation, Conceptualization. **Ganesh Desai Ramakrishna:** Writing – original draft, Visualization, Validation, Software, Methodology, Formal analysis, Data curation, Conceptualization. **Huixuan Wu:** Writing – review & editing, Validation, Supervision, Software, Investigation, Funding acquisition, Formal analysis. **Wei Guo:** Writing – review & editing, Supervision, Funding acquisition.

Declaration of competing interest

The authors declare the following financial interests/personal relationships which may be considered as potential competing interests: Mohammad Mobin Bakhshi reports financial support was provided by U. S. Army Research Office, U.S. Department of Energy, National Science

Foundation. If there are other authors, they declare that they have no known competing financial interests or personal relationships that could have appeared to influence the work reported in this paper.

Acknowledgments

This work is supported byU.S. Department of Energy, United States under Grant NoDE-SC0020113. Research was conducted at theNational High Magnetic Field Laboratory, United States, which is supported byNational Science Foundation, United States Cooperative Agreement NoDMR-2128556 and the State of Florida. Additional support was provided by the U.S. Army Research Office under Grant No W911NF-25-1-0139.

Data availability

Data will be made available on request.

References

[1] Anand. Patel, Heat exchangers in industrial applications: efficiency and optimization strategies, Int. J. Eng. Res. Technol. (ijert) 09 (2023), https://doi.org/10.17577/IJERTV12IS090003, 12.
[2] Gyohoon Geum, et al., Thermal performance analysis of heat pipe heat exchanger for effective waste heat recovery, Int. Commun. Heat Mass Transf. 151 (2024) 107223, https://doi.org/10.1016/j.icheatmasstransfer.2023.107223.
[3] Mohammad Mobin Bakhshi, Qadir Esmaili, Abas Ramiar, Improved performance of vertical solar still by bio-inspired hybrid wettability condenser surface, Case Stud. Therm. Eng. 64 (2024) 105263, https://doi.org/10.1016/j.csite.2024.105263.
[4] Mohammadreza Abbaspour, Qadir Esmaili, Abas Ramiar, A numerical and experimental investigation of the impact of wire mesh on vertical solar still, Case Stud. Therm. Eng. 61 (2024) 105106, https://doi.org/10.1016/j.csite.2024.105106.
[5] Heba Alzaben, S.A. Marzouk, Critical review of heat transfer advancements using bubbles injection in heat exchangers, Renew. Sustain. Energy Rev. 226 (2026) 116395, https://doi.org/10.1016/j.rser.2025.116395.
[6] Mikołaj Matuszczak, et al., Experimental comparison of finned tube heat exchangers for heat rejection under natural convection conditions, Int. Commun. Heat Mass Transf. 154 (2024) 107461.
[7] S.A. Marzouk, et al., Experimental and numerical investigation of a novel fractal tube configuration in helically tube heat exchanger, Int. J. Therm. Sci. 187 (2023) 108175, https://doi.org/10.1016/j.ijthermalsci.2023.108175.
[8] Brajesh Kumar Ahirwar, Arvind Kumar, Effect of wire coil inserts on heat transfer enhancement and fluid flow characteristics of a double-pipe heat exchanger, J. Therm. Anal. Calorim. 7 (2024) 3027–3042, https://doi.org/10.1007/s10973-024-12889-z, 149.
[9] Sagar D. Shelare, Kapil R. Aglawe, Pramod N. Belkhode, A review on twisted tape inserts for enhancing the heat transfer, Mater. Today: Proc. 54 (2022) 560–565, https://doi.org/10.1016/j.matpr.2021.09.012.
[10] Y. Zhang, J. Jiang, S. Fu, J. Liu, X. Liu, L. Feng, A. Li, P. Liu, Y. Chen, Q. Cai, Numerical study on flow characteristics of spiral channel with coiled wire, Processes 13 (3) (2025), https://doi.org/10.3390/pr13030667.
[11] W. Qiu, P. Samruaisin, V. Chuwattanakul, N. Maruyama, M. Hirota, S. Eiamsa-ard, Evaluation of heat transfer performance of a heat exchanger tube mounted with an I-rib twisted tape and twisted winglets, Sci. Rep. 15 (1) (2025) 37047, https://doi.org/10.1038/s41598-025-20806-z.
[12] S.S. Mousavi Ajarostaghi, M. Zaboli, H. Javadi, B. Badenes, J.F. Urchueguia, A review of recent passive heat transfer enhancement methods, Energies 15 (3) (2022) 986, https://doi.org/10.3390/en15030986.
[13] Chenyu Pei, et al., High-efficient cooling from a counter-flow microchannel heat sink with sinusoidal wave walls for high-performance electronic devices, Energy (2025) 138479, https://doi.org/10.1016/j.energy.2025.138479.
[14] Heba Alzaben, et al., Heat transfer enhancement in double tube heat exchanger by wire inserts, Int. J. Heat Fluid Flow 117 (2026) 110093, https://doi.org/10.1016/j.ijheatfluidflow.2025.110093.
[15] W. Liu, Z. Yang, B. Zhang, P. Lv, Experimental study on the effects of mechanical vibration on the heat transfer characteristics of tubular laminar flow, Int. J. Heat Mass Transf. 115 (2017) 169–179, https://doi.org/10.1016/j.ijheatmasstransfer.2017.07.025.
[16] B. Ghorbani, S. Ebrahimi, K. Vijayaraghavan, CFD modeling and sensitivity analysis of heat transfer enhancement of a ferrofluid flow in the presence of a magnetic field, Int. J. Heat Mass Transf. 127 (2018) 544–552, https://doi.org/10.1016/j.ijheatmasstransfer.2018.06.050.
[17] X.-L. Gao, X.-D. Bao, S.-J. Pang, J. Wu, K. Luo, H.-L. Yi, The electrohydrodynamic enhancement of heat transfer on interdigitated electrodes by a charge injection pump, Phys. Fluids 36 (3) (2024), https://doi.org/10.1063/5.0192399.
[18] Z. Rachdi, N. Hnaien, A. Eladeb, B.M. Alshammari, L. Kolsi, H. Dhahri, CFD analysis of heat transfer enhancement in impinging jet array by varying number of jets and spacing, Sci. Rep. 15 (1) (2025) 3023, https://doi.org/10.1038/s41598-025-86360-w.
[19] P. Naphon, Study on the heat transfer and flow characteristics in a spiral-coil tube, Int. Commun. Heat Mass Transf. 38 (1) (2011) 69–74, https://doi.org/10.1016/j.icheatmasstransfer.2010.10.007.
[20] Zhang, J., and Li, S., "Numerical studies of an eccentric tube-in-tube helically coiled heat exchanger for IHEP-ADS helium purification system," arXiv preprint arXiv:1412.8535, 2014. https://doi.org/10.48550/arXiv.1412.8535.
[21] M. Abdelmagied, Investigation of heat transfer and fluid flow in annular curved tubes in laminar flow using Al2O3–water nanofluid, Discov. Appl. Sci. 6 (12) (2024) 673, https://doi.org/10.1007/s42452-024-06312-3.
[22] K. Sharma, P. Deepu, S. Kumar, Convective heat transfer inside a rotating helical pipe filled with saturated porous media, Heat Transf. Res. 55 (10) (2024), https://doi.org/10.1615/HeatTransRes.2024051673.
[23] N. Nivedita, P. Ligrani, I. Papautsky, Dean flow dynamics in low-aspect ratio spiral microchannels, Sci Rep 7 (2017) 44072, https://doi.org/10.1038/srep44072.
[24] A. Dabestani, M. Kahani, CFD analysis of rotation effect on flow patterns and heat transfer enhancement in a horizontal spiral tube heat exchanger, Case Stud. Therm. Eng. 64 (2024) 105494, https://doi.org/10.1016/j.csite.2024.105494.
[25] M. Kim, A. Borhan, Critical conditions for development of a second pair of Dean vortices in curved microfluidic channels, Phys. Rev. E 107 (5) (2023) 055103, https://doi.org/10.1103/PhysRevE.107.055103.
[26] W.Y. Tey, Y. Asako, N.A. Che Sidik, R.Z. Goh, Governing equations in computational fluid dynamics: derivations and A recent review, Prog. Energy Env. 1 (Jun. 2017) 1–19.
[27] Andrea Cioncolini, Lorenzo Santini, An experimental investigation regarding the laminar to turbulent flow transition in helically coiled pipes, Exp. therm. fluid sci. 4 (2006) 367–380, https://doi.org/10.1016/j.expthermflusci.2005.08.005, 30.
[28] Kubair, V. and Varrier, C.B.S. (1961) Indian institute of chemical engineers, 14: 93.
[29] M. Zeng, W. Tao, A comparison study of the convergence characteristics and robustness for four variants of SIMPLE-family at fine grids, Eng. Comput. 20 (3) (2003) 320–340, https://doi.org/10.1108/02644400310467234.
[30] J.F. Shepherd, C.R. Johnson, Hexahedral mesh generation constraints, Eng. Comput. 24 (2008) 195–213, https://doi.org/10.1007/s00366-008-0091-4.
[31] M.M. Etghani, S.A.H. Baboli, Numerical investigation and optimization of heat transfer and exergy loss in shell and helical tube heat exchanger, Appl. Therm. Eng. 121 (2017) 294–301, https://doi.org/10.1016/j.applthermaleng.2017.04.074.
[32] J. Jayakumar, S.M. Mahajani, J. Mandal, K.N. Iyer, P. Vijayan, CFD analysis of single-phase flows inside helically coiled tubes, Comput. chem. eng. 34 (4) (2010) 430–446, https://doi.org/10.1016/j.compchemeng.2009.11.008.
[33] Rahul Harishchandra Patil, Mariappan Dharmaraj Nadar, Rashed Ali, The influence of Dean Number on heat transfer to newtonian fluid through spiral coils with constant wall temperature in laminar flow, Heat Mass Transf. 5 (2017) 1843–1850, https://doi.org/10.1007/s00231-016-1937-8, 53.
[34] R.L. Webb, Performance evaluation criteria for use of enhanced heat transfer surfaces in heat exchanger design, Int. J. Heat Mass Transf. 24 (4) (1981) 715–726, https://doi.org/10.1016/0017-9310(81)90015-6.
[35] Brajesh Kumar Ahirwar, Arvind Kumar, An in-depth numerical and experimental analysis of wire coil inserts: enhancing thermal performance and fluid flow characteristics in double pipe heat exchangers, J. Therm. Anal. Calorim. 149 (2024) 14057–14081, https://doi.org/10.1007/s10973-024-13622-6, 23.
[36] Hamed Sadighi Dizaji, Samad Jafarmadar, Farokh Mobadersani, Experimental studies on heat transfer and pressure drop characteristics for new arrangements of corrugated tubes in a double pipe heat exchanger, Int. J. Therm. Sci. 96 (2015) 211–220, https://doi.org/10.1016/j.ijthermalsci.2015.05.009.
[37] J.S. Jayakumar, et al., Experimental and CFD estimation of heat transfer in helically coiled heat exchangers, Chem. Eng. Res. Des. 3 (2008) 221–232, https://doi.org/10.1016/j.cherd.2007.10.021, 86.